JOURNAL OF MATERIALS SCIENCE 30 (1995) 5705–5710

Properties of Er^{3+}-doped phosphate glasses and glass fibres and efficient infrared to visible upconversion

YA-LIN LU, NAI-BEN MING
National Laboratory of Solid State Microstructures, Nanjing University, and Center for Advanced Studies in Science and Technology of Microstructures, Nanjing 210093, People's Republic of China

Some thermomechanical properties such as expansion, transition temperature and high-temperature viscosity of phosphate glasses with different P_2O_5 and BaO compositions have been measured. Absorption and fluorescence spectra of the phosphate glasses with different Er^{3+} doping have also been measured. The Er^{3+} doping concentration with respect to the maximal fluorescence intensity is 0.75 mol %. The attenuation of the fibre at a wavelength of 1.53 μm is 12.8 db m^{-1}. Upconversion of 1.064 μm Nd : YAG laser pulses into intense green 547 and 667 nm light in the 0.75 mol % Er^{3+}-doped phosphate glass fibre has been achieved. The output power of the two fluorescence signals of green 547 nm and red 667 nm are 178 and 42 μW, respectively, with an upconversion efficiency of 1.78×10^{-2} % and 4.2×10^{-3} % respectively.

1. Introduction

Certain lanthanide-doped glass fibres which can be photoexcited to emit light at wavelengths shorter than that of exciting radiation, have been developed over the past three decades [1–4]. This frequency upconversion can arise from a multiphoton absorption mechanism [4]. Excited-state absorption (ESA), addition of photons by energy transfer (ET), and photon avalanche absorption (PAA) [5] are three main processes of frequency upconversion [4]. Glasses exhibiting efficient infrared to visible upconversion have many important applications, such as display, data storage, optical communications, and ultrashort pulse generation in the visible and violet regions [6, 7]. The upconversion properties of various lanthanide ions in a wide range of glassy and crystalline hosts, such as silica glass [8, 9] and heavy metal fluoride and choloride glasses [10–14], have been extensively examined, but the infrared to visible upconversion in phosphate host glass has received little attention [15]. Current interest in high-average short-wavelength upconversion fibre lasers has stimulated the development of those glasses with excellent fibre performance and good thermomechanical properties which are good for fibre preparation. In the present work, some basic thermomechanical properties and optical properties of phosphate glasses with different BaO compositions have been measured. A glass composition, which is suitable for the fibre host glass, has been determined. By using the composition, phosphate glasses with different Er^{3+}-doping concentrations have been prepared. The relationship between fluorescence intensity and Er^{3+} ions concentration have been measured. Concentration quenching was observed when the Er^{3+} concentration exceeds 0.75 mol %. Fibres drawn from this 0.75 mol % Er^{3+}-doped glasses have been used to measure its attenuation property. Efficient infrared to visible upconversion has also been performed in a 45 cm long 0.75 mol % Er^{3+}-doped phosphate fibre.

2. Experimental procedure

2.1. Preparation of the host phosphate glasses

Two series of glasses, with P_2O_5 concentrations of 50 mol % (series A) and 56 mol % (series B), were prepared. To enhance the durability of the glass, 7.0 mol % Al_2O_3 was introduced, as it does not affect the glass's fluorescence lifetime [16]. Likewise, 1.0 mol % PbO was added to improve the optical properties of glass. In series A and B, as listed in Table I, the BaO composition varies from 0.5–40.5 mol % and from 0.5–30.5 mol %, respectively, at intervals of 5.0 mol %. To prepare these phosphate glasses, mixtures of starting oxide materials were melted in quartz crucibles at about 1150 °C. Oxygen was passed through the furnace to eliminate any water impurities. The glass melts were cast into iron moulds at temperature of about 950 °C, and then were annealed in a 500 ° C annealing furnace. The glasses were gradually cooled from 500 °C to room temperature at a cooling rate of 15 °C h^{-1}.

0022–2461

TABLE I The phosphate glass compositions (mol %)

Sample	P_2O_5	BaO	Li_2O	K_2O	Na_2O
A1	50.0	0.5	20.0	20.0	1.5
A2	50.0	5.5	17.5	17.5	1.5
A3	50.0	10.5	15.0	15.0	1.5
A4	50.0	15.5	12.5	12.5	1.5
A5	50.0	20.5	10.0	10.0	1.5
A6	50.0	25.5	7.5	7.5	1.5
A7	50.0	30.5	5.0	5.0	1.5
A8	50.0	35.5	2.5	2.5	1.5
A9	50.0	40.5	0.0	0.0	1.5
B1	56.0	0.5	17.5	17.5	0.5
B2	56.0	5.5	15.0	15.0	0.5
B3	56.0	10.5	12.5	12.5	0.5
B4	56.0	15.5	10.0	10.0	0.5
B5	56.0	20.5	7.5	7.5	0.5
B6	56.0	25.5	5.0	5.0	0.5
B7	56.0	30.5	2.5	2.5	0.5

2.2. Measurement of physical properties

The as-prepared phosphate glasses (series A and B) were cut to the size of $6 \times 6 \times 50\,mm^3$, and were finely polished. The glass transition temperature can be obtained both from thermal expansion experiments or from DTA experiments. DTA experiments were performed by using a Rigaku Pct-10A thermoanalyser. The heating rate during the DTA experiment was controlled at about $10\,^{\circ}C\,min^{-1}$. The variation of viscosity with temperature was recorded using a rotational high-temperature viscometer. The absorption spectra in the range 300–1600 nm of the glasses were recorded with a Perkin–Elmer model Lambda-9 full-spectral spectrophotometer. Fluorescence spectra of the Er^{3+}-doped phosphate glass were measured by a grating monochromator. A xenon lamp was used as a light source, and a GDB-240 photomultiplier tube as a detector. The fluorescence spectra were recorded with an X–Y recorder.

2.3. Preparation of the phosphate glass fibres

Fibre preforms were prepared by a rotational casting method [17]. The cladding glass melt (1000 °C) was poured into a 15 cm long cylindrical iron mould, preheated to 400 °C, which rotated at speeds ≥ 3000 rev. min^{-1}. A highly concentric phosphate cladding glass tube, whose inner diameter can be precisely controlled by the initial volume of injected glass melt, was thus obtained. No bubbles were observed. The core phosphate glass was next transferred into the tube by pouring the core glass melt down a phosphate glass rod in order to avoid bubble formation. The as-prepared preforms were drawn into fibres using a resistance ring furnace with a localized heat zone 8 cm long. The drawing temperature was set at $650 \pm 5\,^{\circ}C$.

2.4. Measurements of attenuation and upconversion in the phosphate glass fibre

Attenuation spectrum in the range 1200–1600 nm of the Er^{3+}-doped fibre was measured using a 40 W WBr lamp as a light source. The light first passed through a grating monochromator and then was focused into the fibre. The output signals from the fibre were amplified by a lock-in multiplifier. The results were processed with a computer. The cut-off method was used in our attenuation measurement of the fibre.

Upconversion experiments were performed on this Er^{3+}-doped phosphate glass fibre. A Q-switched and mode-locked Nd: YAG laser was used as a excitation source. The laser delivered about 100 ps mode-locked pulses at a repetition rate of 100 MHz, modulated by a 1.2 KHz frequency Q-switching. The laser's maximal average output powers were 2 W at wavelength of 1.064 μm. The output light of the laser was first beam-split. One beam of the light was used for power monitoring; the other beam was focused into the fibre by a ×10 objective lens. The output light from the fibre's other end was then focused into a monochromator. The emission spectra were recorded with the monochromator.

3. Results and discussion

3.1. Thermomechanical properties

These glasses, which have high stimulated emission cross-section, high quenching concentration and excellent thermo-mechanical properties, are required for good laser action. For a fibre laser, both emission characteristics and thermomechanical properties of the host glass are important. Low glass transition temperature, low expansion and high viscosity are beneficial for fibre preparation. In phosphate glasses, it is well known that P_2O_5 is a network former, whereas BaO is a modifier. Thus they certainly have great improvement on the glass's thermomechanical properties.

Fig. 1 shows expansion variation with BaO composition of series A and B. Series B glasses have lower expansion than that of series A. This shows that high P_2O_5 content corresponds to low expansion. The expansion coefficient of the two glass series decreases as the BaO content increases. Thus, high P_2O_5 and BaO contents are beneficial to obtain low-expansion host material for optical fibres. The transition temperature of the phosphate glass can be obtained from both the measured expansion coefficient curves and the measured DTA curves. Their results coincided well.

Fig. 2 shows the glass transition temperature variation with BaO content of both series, measured from DTA experiments. Series B glasses have a relatively higher transition temperature, T_g, than that of series A glasses. When the modifier BaO content increases, the characteristic temperature, T_g, increases in both series A and B. This result provides a wider fibre-forming range in the phosphate system during fibre drawing. Fig. 3 shows the relationship between log viscosity and temperature for four samples, A2, A7 and B2, B7, as listed in Table I. According to the general viscosity formula.

$$\log\eta = \alpha + \beta/T \quad (1)$$

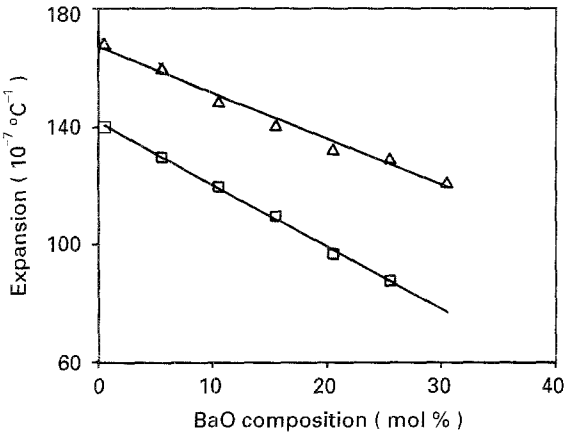

Figure 1 Expansion coefficient variation with BaO content: (△) series A, (□) series B.

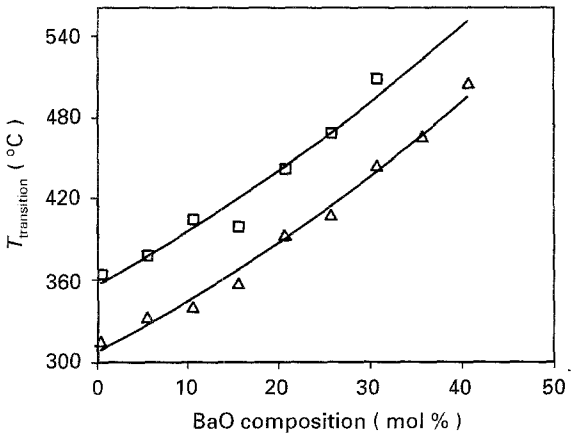

Figure 2 Transition temperature variation with BaO content: (△) series A, (□) series B.

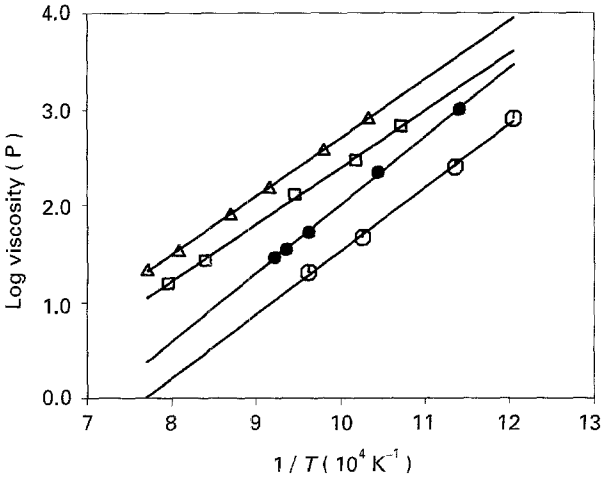

Figure 3 The relationship between log viscosity and temperature: (△) B7, (□) B2, (●) A7, (○) A2.

where $\beta = \Delta\mu/K$, $\Delta\mu$ is the viscous activation energy of the glass, α is a constant relevant to the glass, K is the Boltzman constant, and T the temperature. Thus from Fig. 3, we can calculate the activation energy of the glass, $\Delta\mu$, α and β, which are shown in Table II. From Fig. 3, high P_2O_5 and BaO contents would increase the high-temperature viscosity of the glass and thus is beneficial for fibre-drawing.

TABLE II Activation energy and relevant constants

Sample	$\Delta\mu$ (10^{-19} J)	α	β (10^3 K)
A2	2.20	− 5.30	6.95
A7	2.30	− 5.24	7.10
B2	1.90	− 3.50	6.15
B7	1.95	− 3.40	6.10

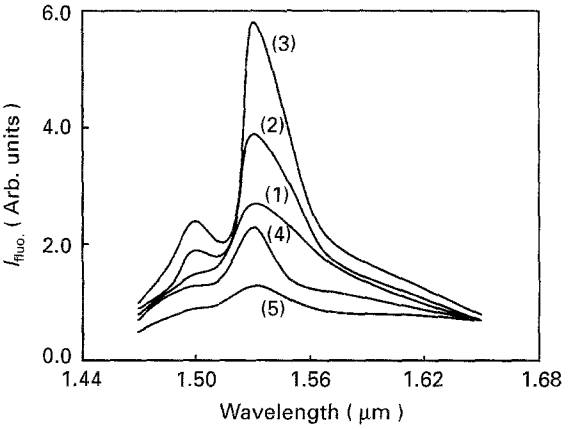

Figure 4 Fluorescence spectra of the Er^{3+}-doped phosphate glasses measured at room temperature. (1) 0.05 mol %, (2) 0.35 mol %, (3) 0.65 mol %, (4) 0.95 mol %, (5) 1.25 mol %.

According to the thermomechanical properties of the glass, the composition, P_2O_5 (56.0 mol %), BaO (15.5 mol %), Li_2O (10.0 mol %), Na_2O (0.5 mol %), K_2O (10.0 mol %), Al_2O_3 (7.0 mol %), and PbO (1.0 mol %) in molar amounts, was chosen for the fibre host glass composition in further experiments.

3.2. Absorption and fluorescence properties

The phosphate glass with above composition was used for fibre cladding glass. Further doping of erbium in above composition was used for the required fibre core glasses. The doped Er^{3+} ion concentrations were from 0.05–1.25 mol % at intervals of 0.3 mol %. Fig. 4 shows the fluorescence spectra in the vicinity of 1.53 μm of the above five as-prepared Er^{3+}-doped phosphate glasses. The relationship between fluorescence intensity and Er^{3+} concentration is shown in Fig. 5. The maxima of fluorescence intensity occurred at an Er^{3+} concentration of about 0.75 mol %. Above this concentration, the fluorescence intensity decreased due to a concentration quenching effect. Thus the glass with a doping concentration of 0.75 mol % Er^{3+} was chosen for core glass in further experiments. Fig. 6 shows the absorption spectrum of the 0.75 mol % Er^{3+}-doped phosphate glass in the wavelength range 300–1600 nm measured at 300 K. The electronic levels reached from the $^4I_{15/2}$ ground-state level can be identified from the recorded absorption spectrum and are listed in Table III. From the recorded absorption spectrum and the fluorescence spectra, the stimulated emission cross-sections, σ, the spontaneous emission probability, A_{ij}, and the effective fluorescence linewidth, $\Delta\lambda_{eff}$, can be calculated

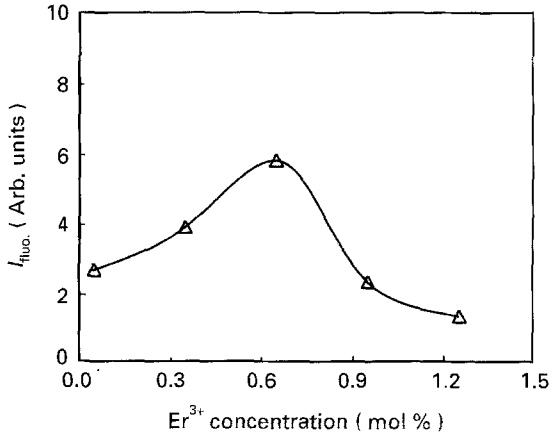

Figure 5 The relationship between fluorescence intensity and Er^{3+} ion concentration.

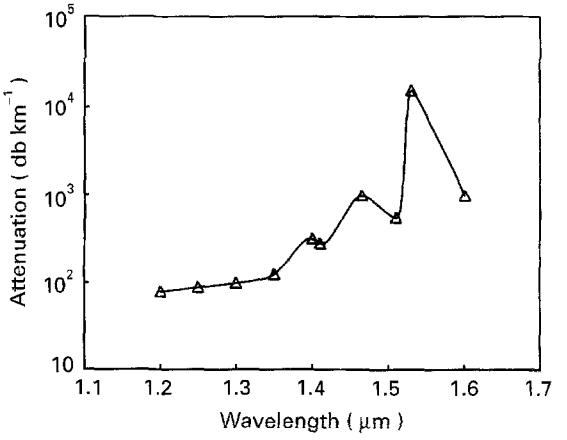

Figure 7 Attenuation spectrum of the Er^{3+}-doped phosphate glass.

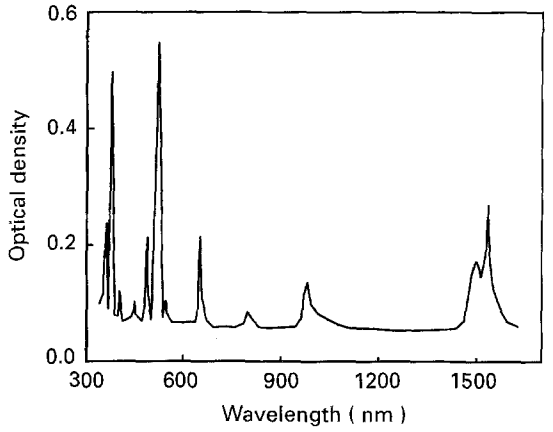

Figure 6 Absorption spectra in 0.75 mol % Er^{3+}-doped phosphate glass measured at 300 K.

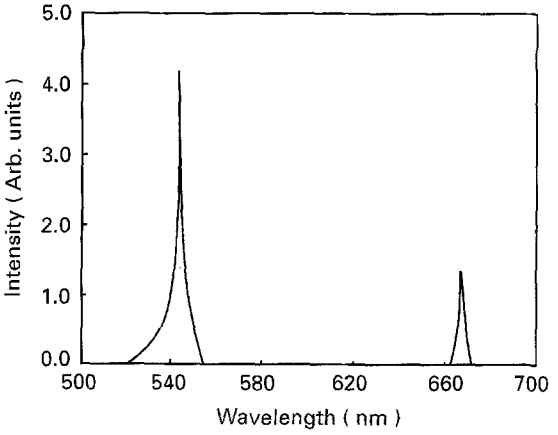

Figure 8 Upconversion luminescence spectra of the Er^{3+}-doped phosphate glass fibre.

TABLE III Electronic levels reached from the $^4I_{15/2}$ ground-state levels in 0.75 mol % Er^{3+}-doped phosphate glass

$E(cm^{-1})$	Level	$E(cm^{-1})$	Level
27501	$^2G_{9/2}$	19275	$^2H_{11/2}$
26525	$^4G_{11/2}$	18437	$^4S_{3/2}$
24667	$^2H_{9/2}$	15394	$^4F_{9/2}$
22625	$^4F_{3/2}$	12547	$^4I_{9/2}$
22242	$^4F_{5/2}$	10235	$^4I_{11/2}$
20559	$^4F_{7/2}$	6524	$^4I_{13/2}$

TABLE IV Some characteristic emission parameters of the Er^{3+}-doped phosphate glass

A_{ij} (s^{-1})	$\Delta\lambda_{eff}$ (nm)	σ (10^{-21} cm^2)
172	60.2	9.0

[18–21]. The stimulated emission cross-section for the $^4I_{13/2}$–$^4I_{15/2}$ transition was calculated using the modified Deutschbein method [22], from the measured absorption intensity of various absorption bands and the effective linewidth of the 1.53 μm fluorescence emission band. The results are listed in Table IV. The results show that the phosphate glass has good properties for application in a fibre laser.

3.3. Attenuation and infrared to visible upconversion

The attenuation spectrum in the wavelength range 1200–1600 nm of the fibre is shown in Fig. 7. The attenuation curve is very similar to the results of Townsend *et al.* [23]. The attenuation of the fibre is of the same order as their results. At a wavelength of 1.53 μm, the attenuation of the fibre is about 12.8 db m^{-1}, which is almost the same as their result of about 10.2 db m^{-1} [23]. The results show that the 0.75 mol % Er^{3+}-doped phosphate fibre drawn with the above procedure is of good optical quality.

Upconversion luminescence spectra were measured in a 45 cm long fibre with an outer diameter if 100 μm in which the core diameter is about 68 μm. The numerical aperture (NA) of the fibre is about 0.155. The luminescence spectra in the range 450–700 nm were measured with 1.064 μm excitation, as shown in Fig. 8. The average output power of the laser is about 1 W. In the visible region there are two signals emanating from the fibre: one is a red light peaked at 667 nm with a nearly 8 nm bandwidth spectrum; the other is green light peaked at 547 nm with a 5.5 nm bandwidth spectrum and asymmetrical towards high frequencies. The 667 nm red signal was relatively weak, whereas the 547 nm green light was very intense. In our experiments, when the average infrared excitation power is

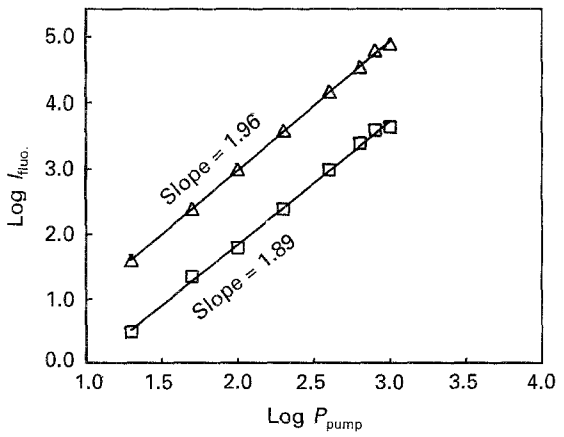

Figure 9 Logarithmic linear relationship between fluorescence intensity and excitation power: (Δ) 547 nm, (□) 667 nm.

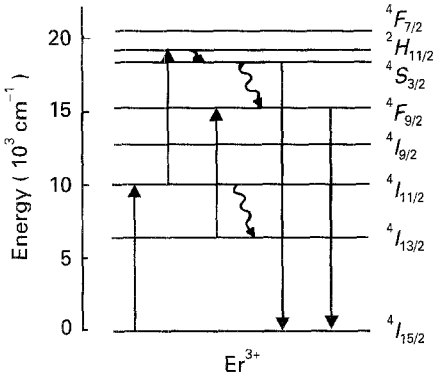

Figure 10 Er^{3+} energy level diagram in the Er^{3+}-doped phosphate glass.

1 W, the output powers of the two 547 and 667 nm visible bands are 178 and 42 μW, respectively. Thus the upconversion efficiencies of the two bands are 1.78×10^{-2}% and 4.2×10^{-3}%, respectively. They are slightly higher than those which were obtained in Er^{3+}-doped silica fibre [9]. In their experiments, three fluorescence bands, 467, 546 and 667 nm, were obtained in a 40 cm long fibre with a 1.064 μm excitation. Their corresponding upconversion efficiencies were 4×10^{-4}%, 1×10^{-2}% and 3×10^{-3}%, respectively. In our experiments, no 467 nm blue signal was measured.

Fig. 9 shows the variation of fluorescence intensity of the two bands with the pumping power. A typical logarithmic linear relationship between fluorescence intensity and excitation power is obtained. For the line corresponding to 547 nm green light, its slope is 1.96 and nearly equals 2. This slope confirms that the generation of 547 nm green light is caused by two-photon absorption fluorescence. Fig. 10 shows the energy level diagram of Er^{3+}-doped phosphate glass. Under the excitation of a 1064 nm laser, Er^{3+} ions were excited from ground-state level $^4I_{15/2}$ to $^2H_{11/2}$ through two-photon absorption. The process includes the ground-state absorption (GSA) ($^4I_{15/2}\rightarrow{}^4I_{11/2}$) and the excited-state absorption (ESA) ($^4I_{11/2}\rightarrow{}^2H_{11/2}$). Then those Er^{3+} ions at the $^2H_{11/2}$ level might decay non-radiatively to the substable level $^4S_{3/2}$ through multiphonon relaxation (MPR). Thus a radiative transition from the $^4S_{3/2}$ and terminating on the ground level $^4I_{15/2}$ gives to the most intense green 547 nm fluorescence, as shown in Fig. 10. In Fig. 9, the slope of the line corresponding to 667 nm red light is 1.89 and is slightly smaller than 2. The result also confirms that the generation of 667 nm light is primarily caused by two-photon absorption fluorescence. Er^{3+} ions were first excited to $^2H_{11/2}$ through two-photon absorption. Then they decay to the $^4S_{3/2}$ level and further decay to the $^4F_{9/2}$ level through MPR. Thus the red 667 nm signal is the $^4F_{9/2}\rightarrow{}^4I_{15/2}$ upconversion fluorescence. Because the slope of the line is smaller than 2, it shows the complexity of this upconversion process. One of the possible processes, as shown in Fig. 10, may contribute to the $^4F_{9/2}$ level population. The process is that those Er^{3+} at the level $^4I_{11/2}$ may decay non-radiatively to level $^4I_{13/2}$ through MPR after the excitation from the ground-state level $^4I_{15/2}$, and then transition from $^4I_{13/2}$ to the $^4F_{9/2}$ level through absorption of another infrared photon. Further work on our experiments will involve use of a continuous wave 980 nm laser diode excitation. The use of a 980 nm pump should be more practical and more efficient because the $^4I_{11/2}\rightarrow{}^4I_{15/2}$ absorption transition of the Er^{3+} ion is in the vicinity of 980 nm, as shown in Fig. 6.

4. Conclusion

Thermomechanical properties, such as expansion, high-temperature viscosity, and the glass transition temperature, of phosphate glasses with different P_2O_5 and BaO contents have been measured. High P_2O_5 content will introduce low thermal expansion, high transition, and high-temperature viscosity in the phosphate glass system, whereas high BaO content will lead to the decrease of thermal expansion, an increase of the glass transition temperature, and an increase of high-temperature viscosity. The phosphate glasses with different Er^{3+}-doping concentrations have been used to measure the fluorescence spectra of the glass. The maximal fluorescence intensity occurred at an Er^{3+} concentration of 0.75 mol %. When the doping of erbium exceeds 0.75 mol %, the fluorescence intensity decreases due to the effect of concentration quenching. The attenuation spectra of the fibre drawn from 0.75 mol % erbium-doped phosphate glasses has been measured. Upconversion of 1.064 μm Nd:YAG laser pulses into intense green 547 nm and red 667 nm light in the fibre has been achieved. The output power of the fluorescence signals are 178 and 42 μW, respectively, with an average excitation power of 1 W.

Acknowledgement

This work was supported by a Ke-Li Fellowship.

References

1. N. BLOEMBERGEN, *Phys. Rev.* **2** (1959) 84.
2. M. R. BROWN and W. A. SHAND, *Phys. Rev. Lett.* **11** (1963) 366.
3. *Idem, ibid.* **12** (1964) 367.

4. F. AUZEL *Proc. IEEE* **61** (1973) 758.
5. W. E. CASE, M. E. KOCH and A. W. KUENY, *J. Lumin.* **45** (1990) 351.
6. P. XIE and S. C. RAND, *Optics Lett.* **17** (1992) 1116.
7. T. HERBERT, R. WANNEMACHER, R. M. MACFARLANE and W. LENGTH, *Appl. Phys. Lett.* **60** (1992) 2592.
8. P. URQUAHRT, *IEE Proc. J* **135** (1988) 385.
9. Y. M. HUA and Y. X. CHEN, *Chin. J. Lasers* **19** (1992) 228.
10. E. W. J. L. OOMEN, P. M. T. LEGALL and A. M. A. VANDONGEN, *J. Lumin.* **46** (1990) 353.
11. M. A. CHAMARRO and R. CASEA, *ibid.* **46** (1990) 59.
12. D. C. YEH, W. A. SIBLEY, I. SCHNEIDER, R. S. AFZAL and I. AGGARWAL, *J. Appl. Phys.* **69** (1991) 1648.
13. ALI GHARAVI and GARY L. MCPHERSON, *Appl. Phys. Lett.* **61** (1992) 2635.
14. SENG C. GOH, *J. Non-Cryst. Solids* **161** (1993) 227.
15. P. LAPORTA, S. LONGHI, S. TACCHEO, O. SVEITO and G. SACCHI, *Electron. Lett.* **28** (1992) 2067.
16. Y. S. JIANG, S. B. JIANG and Y. Y. JIANG, *J. Non-Cryst. Solids* **112** (1989) 286.
17. D. C. TRAN, C. F. FISHER and G. H. SIGEL, Electron. Lett. **18** (1982) 657.
18. R. R. JACOBS and M. J. WEBER, *IEEE J. Quant. Electron.* **QE-12** (1976) 102.
19. Y. L. LU and N. B. MING, *Opt. Commun.* **115** (1995) 110.
20. B. R. JUDD, *Phys. Rev.* **127** (1962) 750.
21. A. A. KAMINSKII, "Laser Crystals" (Springer, 1981) p. 154.
22. S. E. STOKOWSKI, Laser Program Annual Reports, Lawrence Livermore National Laboratory, Vol. 2 (1978) p. 7. 52.
23. J. E. TOWNSEND. S. B. POOLE and D. N. PAYNE, *Electron. Lett.* **23** (1987) 329.

Received 18 July 1994
and accepted 7 June 1995